[Supplementary material]

Optically stimulated luminescence profiling and dating of earthworks: the creation and development of prehistoric field boundaries at Bosigran, Cornwall

Soetkin Vervust[1,2,*], Tim Kinnaird[3], Peter Herring[4] & Sam Turner[1]

[1] *McCord Centre for Landscape, Newcastle University, UK*

[2] *Vrije Universiteit Brussel, Brussels, Belgium*

[3] *School of Earth and Environmental Sciences, University of St Andrews, UK*

[4] *Cornwall Council, Truro, UK*

[*] *Author for correspondence: ✉ soetkin.vervust@newcastle.ac.uk*

Table S1. Sample descriptions.

Field Profile ID	**CERSA lab code**	**Depth (m)**	**Context / sedimentological descriptions**
Site 1: Halldrine Croft co-axial field-system; based on results of West Penwith field survey assumed to be Middle Bronze Age (not re-used in later period); 1500–1000 BC			
P1 OSL1	285	0.48	[001], dark-brown, sandy humic soil with granules (approx. 5mm) of weathered granite
P1 OSL2	286	0.50	[003], orange-brown loamy-clay with some sand and small granite granules
Site 3: stone-faced lynchet forming the boundary of a field 80m south-east of the easternmost courtyard house in the western hamlet at Bosigran; based on results of West Penwith field survey assumed to be Late Iron Age (re-used in medieval and post-medieval periods); 0–500 AD			
P2 OSL1	288	0.35	[005], earth bank
P2 OSL2	289	0.70	[007], greyish-brown silt-clay-loam
P2A OSL1	300	1.04	[022], light greyish-brown sandy loam
P2A OSL2	301	1.12	[023], grey sandy silt loam, extends to the south beneath [019] and [018]
P2A OSL3	302	1.27	[027], brown silty loam
P2A OSL4	303	0.50	[025], brown loam

S1. Luminescence screening measurements – relative in the field; calibrated in the laboratory.

All sediments were appraised using portable OSL equipment in the field. This provided the first preliminary assessment of luminescence behavior, and the means to generate relative luminescence stratigraphies. Details on the SUERC portable OSL reader are provided in Sanderson and Murphy (2010). The measurement cycle involved an interleaved sequence of instrument dark count, IRSL and OSL, similar to that described by Sanderson and Murphy (2010), and utilised by Kinnaird *et al*. (2017a). This method allows for the calculation of IRSL and OSL net signal intensities and IRSL and OSL depletion indices (table S2).

Mineral preparation procedures similar to those used by Burbidge *et al*. (2007) and Kinnaird *et al*. (2017a) were used to extract HF-etched 'quartz' from each of the profiled samples. Paired aliquots of 'quartz' were subjected to a simplified four step SAR procedure (with repeat and zero doses) to obtain estimates of stored dose (Gy) and sensitivity (counts per Gy; table S2), and assess apparent dose and sensitivity distributions (columns 10 & 11). Apparent ages were also determined for the 'calibrated' dataset, by combining the extrapolated stored dose estimates with the dose rates estimated for each position (cf. Muñoz-Salinas *et al*. 2014; Kinnaird *et al*. 2017a, b; Turner *et al*. 2018). The close proximity of the full dating and profiling samples, and the uniformity of the dose rates, justify this approach. The total dose rates for the profiling samples were either estimated on the basis of the adjacent dating sample, or through interpolating dose rates from enclosing dating samples (S5). Apparent age estimates were then calculated combining these extrapolated dose estimates with the dose rates for each position. These values were used to generate Figures 4, 5 and 6 in the main text.

Table S2. Results from field- and laboratory luminescence screening on bulk sediments from Bosigran profiles 1 and 2.

Field ID	Depth (m)	Context	Field OSL measurements				Laboratory calibrated OSL measurements					
			IRSL		OSL		OSL					
			Net signal intensities /counts	Depletion ratio	Net signal intensities /counts	Depletion ratio	Stored dose (Gy)		Sensitivity / counts (Gy^{-1})		Apparent dose (Gy)	Sensitivity / counts (Gy^{-1})
P1/1	0.41	1	58 830±250	1.33±0.01	1 378 550±1180	1.98±0.01	17.3±0.6	14.3±0.4	23 470±150	18 860±140	15.8±1.5	21 170±2300
P1/2	0.45	1	67 530±260	1.34±0.01	1 376 350±1180	2.23±0.01	23.8±0.6	27.1±0.9	10 660±100	13 900±120	25.4±1.7	12 280±1620
P1/3	0.55	3	137 740±380	1.36±0.01	641 230±810	1.59±0.01	58.2±3.8	27.8±1	2740±50	3640±60	43±15.2	3190±450
P1/4	0.14	1	26 000±170	1.37±0.02	1 607 340±1270	2.23±0.01	5.2±0.1	4.4±0.1	99 100±310	78 560±280	4.8±0.4	88 830±10 270
P1/5	0.23	1	42 440±210	1.38±0.01	1 644 500± 280	2.34±0.01	-	-	-	-	-	-
P1/6	0.28	1	43 510±220	1.35±0.01	1 492 230± 220	2.16±0.01	11.5±0.3	11.9±0.4	35 640±190	24 670±160	11.7±0.2	30 150±5490
P1/7	0.36	1	58 020±250	1.31±0.01	1 646 660±1290	2.07±0.01	20.2±0.5	21.2±0.6	32 420±180	20 580±140	20.7±0.5	26 500±5920
P1/8	0.41	1	149 650±400	1.36±0.01	2 501 840±1590	2.15±0.01	31.5±1	24.8±0.8	15 180±120	18 230±140	28.1±3.3	16 710±1530
P1/9	0.46	1	700 300±840	1.43±0.01	3 324 950±1830	1.75±0.01	25.3±0.8	32.8±1.3	5210±70	5150±70	29.1±3.7	5180±30
P1/10	0.51	3	241 240±500	1.38±0.01	1 147 560±1080	1.61±0.01	24.6±1.1	18.7±1.3	2500±50	1030±30	21.6±2.9	1770±740
P1/11	0.59	3	180 180±430	1.40±0.01	728 000±860	1.69±0.01	43.4±5.1	56.2±4.2	1350±40	4700±70	49.8±6.4	3030±1670
P1/12	0.64	3	188 820±440	1.30±0.01	677 530±830	1.55±0.01	24.3±1.3	62±3.8	1680±40	5790±80	43.1±18.8	3740±2050
P2/1	0.34	22	9320±100	1.43±0.03	614 220±790	2.52±0.01	3.5±0.1	4.9±0.1	43 810±210	230±230	4.2±0.7	48 990±5190
P2/2	0.38	22	29 980±180	1.44±0.02	935 700±970	2.43±0.01	4.6±0.1	4.9±0.2	107 760±330	230±230	4.8 ± 0.2	80 810±26 950
P2/3	0.43	22	22 800±160	1.49±0.02	864 300±930	2.55±0.01	5±0.1	4.8±0.1	95 040±310	230±230	4.9±0.1	74 450±20 590
P2/4	0.49	22	16 940±140	1.39±0.02	756 750±870	2.39±0.01	4.7±0.1	5.3±0.2	41 620±200	220±220	5±0.3	45 190±3570
P2/5	0.54	22	31 870±180	1.48±0.02	839 660±920	2.32±0.01	5.4±0.2	5.5±0.2	52 080±230	230±230	5.4±0.1	51 760±320
P2/6	0.61	22	38 240±200	1.42±0.01	809 670±900	2.21±0.01	20.1±0.7	6±0.2	58 270±240	200±200	13.1±7	49 740±8520
P2/7	0.73	22	72 420±270	1.40±0.01	852 430±930	2.08±0.01	8.3±0.2	10.9±0.3	67 670±260	220±220	9.6±1.3	58 130±9540
P2/8	0.80	4	223 390±480	1.43±0.01	1 421 770±1200	1.88±0.01	9.4±0.3	28.6±1	77 610±280	240±240	19±9.6	67 980±9630
p2a/10	0.24	18	3270±70	1.37±0.05	222 190±470	2.24±0.01	1.5±0	5.1±0.1	56 810±240	270±270	3.3±1.8	65 560±8750
p2a/11	0.29	18	6200±80	1.43±0.04	343 960±590	2.41±0.01	2.6±0.1	1.4±0	72 540±270	200±200	2±0.6	56 510±16 030
p2a/12	0.45	18	19 940±150	1.44±0.02	938 160±970	2.64±0.01	11±0.3	11.7±0.3	33 010±180	160±160	11.3±0.4	29 950±3060
p2a/13	0.50	19	21 080±150	1.40±0.02	838 710±920	2.20±0.01	18.8±0.5	16.9±0.5	19 340±140	110±110	17.8±1	16 250±3090
p2a/14	0.60	19	28 480±170	1.39±0.02	1 154 310±1080	2.27±0.01	18.5±0.6	21.1±0.7	27 570±170	260±260	19.8±1.3	47 700±20 120
p2a/15	0.70	23	27 620±170	1.40±0.02	93 4410±970	2.25±0.01	23.3±0.8	20.1±0.6	23 860±150	190±190	21.7±1.6	30 130±6260
p2a/16	0.80	23	103 870±330	1.44±0.01	81 7320±910	1.83±0.01	139.1±4.3	76.9±7.3	40 390±200	100±100	108±31.1	25 300±15 090
p2a/17	0.86	27	83 100±290	1.40±0.01	39 7900±630	1.71±0.01	106±3.5	98.9±3.3	13850±120	90±90	102.5±3.5	11 280±2570

p2a/18	0.92	27	209 080±460	1.48±0.01	89 9720±950	1.65±0.01	73.6±5.5	32.5±1.3	8260±90	70±70	53.1±20.5	6550±1720
p2a/19			392 670±630	1.44±0.01	1 917 740±1390	1.65±0.01	-	-	-	-	-	-
p2a/20	0.56	22	4840±80	1.38±0.04	470 470±690	2.37±0.01	6±0.2	5.4±0.1	59 420±240	270±270	5.7±0.3	67 050±7630
p2a/21	0.72	22	7700±100	1.36±0.03	625 530±790	2.36±0.01	6.1±0.2	6.7±0.2	94 820±310	240±240	6.4±0.3	76 730±18 090
p2a/22	0.84	22	13 650±120	1.35±0.02	1 046 860±1030	2.30±0.01	14.1±0.4	15±0.4	84 230±290	240±240	14.5±0.4	71 130±13 100
p2a/23	0.96	22	15 050±130	1.35±0.02	799 520 ± 900	2.26±0.01	18.8±0.6	16.6±0.4	34 300±190	210±210	17.7±1.1	39 580±5280
p2a/24	1.03	22	26 130±170	1.40±0.02	950 790 ± 980	2.37±0.01	19±0.5	21±0.6	27 650±170	140±140	20±1	24 010±3640
p2a/25	1.11	23	35 980±200	1.36±0.01	1 067 940±1040	2.25±0.01	21.5±0.6	21.2±0.7	19 140±140	180±180	21.4±0.1	26 460±7320
p2a/26	1.17	23	53 840±240	1.36±0.01	1 038 430±1020	2.12±0.01	20.2±0.5	21.4±0.6	18550±140	180±180	20.8±0.6	24 720±6170
p2a/27	1.23	27	76 980±280	1.39±0.01	435 060 ± 660	1.59±0.01	113 ± 3.9	54.6±3.1	8890±90	90±90	83.8±29.2	8770±120
p2a/28	1.28	27	132 730±370	1.49±0.01	568 900±760	1.63±0.01	37±1.9	125.3±46.3	3320±60	80±80	81.1±44.1	5200±1880
p2a/29	0.92	26	16 830±130	1. ±0.02	970 840±990	2.37±0.01	11.8±0.3	10.5±0.3	38 470±200	270±270	11.1±0.7	54 660±16 200
p2a/30	0.99	26	18 860±140	1.38±0.02	999 270±1000	2.30±0.01	11.4±0.3	12.3±0.4	48 820±220	270±270	11.8±0.4	61 930±13 110
p2a/31	1.10	27	78 040±280	1.41±0.01	723 850±850	1.97±0.01	70.8±5.5	26.3±0.9	37 000±190	170±170	48.5±22.3	32 770±4230
p2a/32	1.15	27	35 790±190	1.38±0.01	316 580±570	1.88±0.01	88.6±6.9	145.6±23.6	6990±80	80±80	117.1±28.5	6680±310
p2a/33	1.21	27	54 250±240	1.45±0.01	268 050±520	1.73±0.01	37.9±1.7	54.8 ± 3.7	15 470±120	100±100	46.4±8.5	12 850±2610
p2a/34	0.46	22	5740±80	1.54±0.04	514 100±720	2.60±0.01	5.4±0.1	4.4 ± 0.1	41 320±200	210±210	4.9±0.5	42 060±740
p2a/35	0.55	22	5170±80	1.44±0.04	574 780±760	2.40±0.01	3.5±0.1	3.3 ± 0.1	49 740±220	210±210	3.4±0.1	46 500±3240
p2a/36	0.64	25	6140±80	1.39±0.04	576 040±760	2.40±0.01	4.9±0.1	5.5 ± 0.1	60 080±250	260±260	5.2±0.3	63 190±3110
p2a/37	0.74	25	6920±90	1.45±0.04	544 920±740	2.38±0.01	8.1±0.2	6.2±0.2	118 790±340	200±200	7.1±1	79 610±39 180
p2a/38	0.83	25	9900±100	1.46±0.03	747 930±870	2.52±0.01	5±0.1	5.4±0.2	56 520 ± 240	260±260	5.2±0.2	62 820±6300
p2a/39	1.00	25	12 690±120	1.42±0.03	675 300±820	2.34±0.01	5.8±0.2	6.3±0.2	52 410 ± 230	290±290	6.1±0.2	67 600±15 190
p2a/40	1.04	25	12 110±120	1.39±0.03	604 950±780	2.27±0.01	7.8±0.2	6.2±0.2	50 080 ± 220	220±220	7±0.8	48 240±1840

Sample preparation

Sample preparation was undertaken under safe light conditions at the luminescence laboratories at the School of Earth and Environmental Sciences, University of St Andrews. Equivalent dose determinations were undertaken at St Andrews. Dose rate determinations were made at the Environmental Radioactivity Laboratory (ERL) at the School of Biological and Earth Sciences, University of Stirling.

Mineral preparation of quartz

Standard mineral preparation procedures as routinely used in OSL dating were used to extract sand-sized quartz from each sample (cf. Kinnaird *et al*. 2017a). Quartz was extracted from the portion of each sample which had not been exposed to sunlight since burial. The samples were wet-sieved to obtain the 90–250µm size fraction, then treated in 1M hydrochloric acid (HCl) for 10 minutes, followed by 40% Hydrofluoric acid (HF) for 40 minutes, and a further treatment in 1 M HCl for 10 minutes. The HF-etched fractions were then density separated in LST heavy liquids at concentrations of 2.64 and 2.74gcm^{-3}, to obtain concentrates of feldspar (< 2.64gcm^{-3}) quartz (2.64–2.74gcm^{-3}) and heavy minerals (>2.74gcm^{-3}). The quartz concentrates were re-sieved at 150µm; the 150–250µm fractions were dispensed to 10mm stainless steel discs in sets of 20+ aliquots.

Preparation of samples for HRGS

Bulk materials were dried to a constant weight in an oven set at 50°C. Sub-quantities of the dried sediment, weighing approximately 170–180g, were taken and ground by hand to a fine powder using a pestle and mortar. These materials were used to fill 150ml high-density plastic plots for gamma spectrometry. Each pot was sealed with epoxy resin and placed in storage for at least four weeks.

Equivalent dose determinations

All OSL measurements were carried out using a Risø TL/OSL DA-20 automated dating system, equipped with a ^{90}Sr/^{90}Y β-source for irradiation (dose rate at time of measurement, 1.10 Gy/s), blue LEDs emitting around 470nm and infrared diodes emitting around 830nm for optical stimulation. OSL was detected through 7.5mm of Huoya U-340 filter and detected with a 9635QA photomultiplier tube. OSL was measured at 125°C for 60s. The OSL signals, *Ln* and *Lx*, used for equivalent dose (D_e) determinations were obtained by integrating the OSL counts in the first 2.4s and subtracting an equivalent signal taken from the last 9.6s.

D_e determinations were determined using a single-aliquot regenerative dose (SAR) method (Murray & Wintle 2000; Kinnaird *et al*. 2017a), which allows for an independent estimate of D_e to be generated for each aliquot measured. The SAR technique involves making a series of paired measurements of OSL intensity - the *Ln* and *Lx* outlined above, and the response to a fixed test dose, *Tn* and *Tx*. Each measurement is standardised to the test dose response determined immediately after its readout, to compensate for observed changes in sensitivity during the laboratory measurement sequence. D_e values are then estimated using the corrected OSL intensities *Ln/Tn* and *Lx/Tx* and the interpolated dose-response curve.

This was implemented here, using four (to five) regenerative doses (nominal doses of 2.5, 5, 10 and 30 Gy; extended to 60 Gy for CERSA300-303), with additional cycles for zero dose, repeat or 'recycling' dose and IRSL dose. The zero dose point is used to monitor 'recuperation', thermally induced charge transfer during the irradiation and preheating cycle. The repeat dose - a repeat of the initial regeneration dose - is used to calculate the 'recycling ratio', a test of the internal consistency of the growth curve. The IRSL response check is included to assess the magnitude of non-quartz signals. To ensure that there was no dependency of D_e or sensitivity on preheat conditions, five preheat temperatures were explored from 220 to 260°C in 10°C increments.

Data reduction and D_e determinations were made in Luminescence Analyst v.4.31.9. Individual decay curves were scrutinised for shape and consistency. Dose response curves were fitted with an exponential function, with the growth curve fitted through zero and the repeat recycling points. Error analysis was determined by Monte Carlo Stimulation.
Representative OSL decay curves for both the natural and regenerated signals are shown in Figure S1 for CERSA285, together with the corresponding dose response curve.

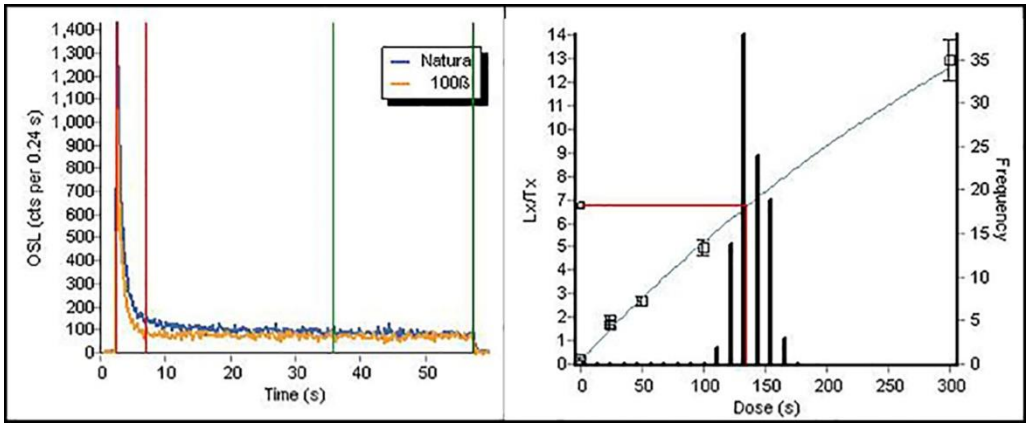

Figure S1. Left) decay curve; right) dose response curve for CERSA285 (aliquot 1).

Equivalent dose distributions

OSL SAR dating utilises extracted quartz from the samples to determine the radiation dose experienced by the sediments since their last zeroing event assumed to be by exposure to light prior to final deposition, the burial dose, *Db*. To obtain a depositional age, it is necessary to reduce each samples D_e distribution to a single *Db*.

Internal consistency of quartz OSL SAR data

Aliquots were rejected from further analysis if they failed sensitivity checks (based on test dose response), SAR acceptance criteria checks, or had significant IRSL response coupled with anomalous luminescence behaviour (Table S3).

Table S3. OSL SAR acceptance criteria, 150–250 micron fractions. Errors provided as standard deviations.

CERSA no.	Sensitivity / counts (Gy^{-1})	Recuperation (%)	Recycling ratio	IR response (%)	Dose recovery
285	2780±2140	0.4±0.2	1.02±0.03	0.1±0.2	0.99±0.02
286	1630±230	0.6±0.8	1.02±0.07	0.2±0.9	0.97±0.03
288	2320±270	1.3±0.3	1.02±0.04	0.1±0.1	1.00±0.03
289	3580±4010	0.8±0.4	1.03±0.02	0.1±0.2	1.03±0.03
300	20 000±38 260	0.9±0.3	1.01±0.03	3.4±2.5	1.02±0.04
301	2750±820	0.6±0.2	1.00±0.03	0.3±0.6	1.01±0.03
302	3910±3350	0.6±0.4	1.02±0.04	2.7±4.3	1.00±0.04
303	2700±530	1.1±0.7	1.02±0.01	0.1±0.1	1.01±0.01

Distribution analysis

The distributions in equivalent dose values, for those aliquots which satisfied the SAR selection criteria, were examined using Kernel Density Estimate (KDE) plots and Abanico plotting methods (Figs S2–S9; Dietze *et al*. 2013)

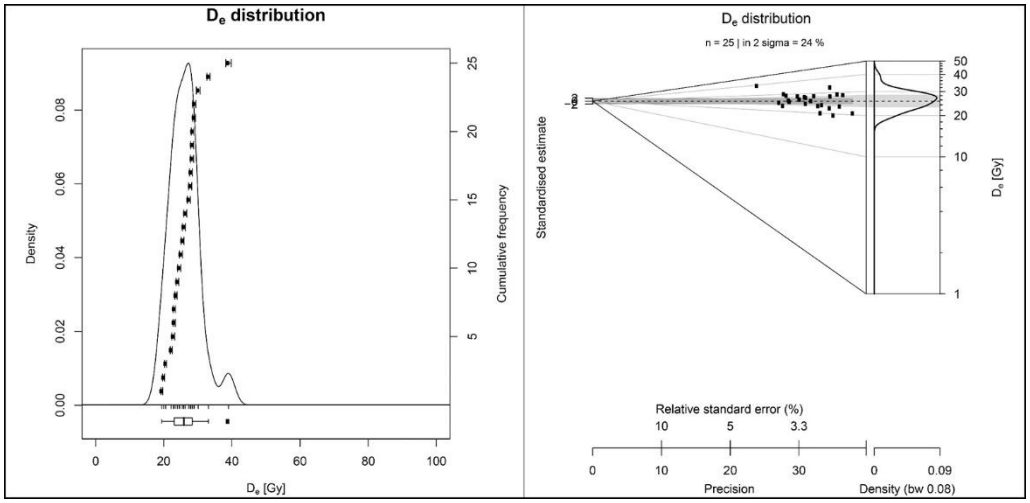

Figure S2. D_e distributions for CERSA285: left) Kernel Density Estimate Plot; right) Abanico Plot.

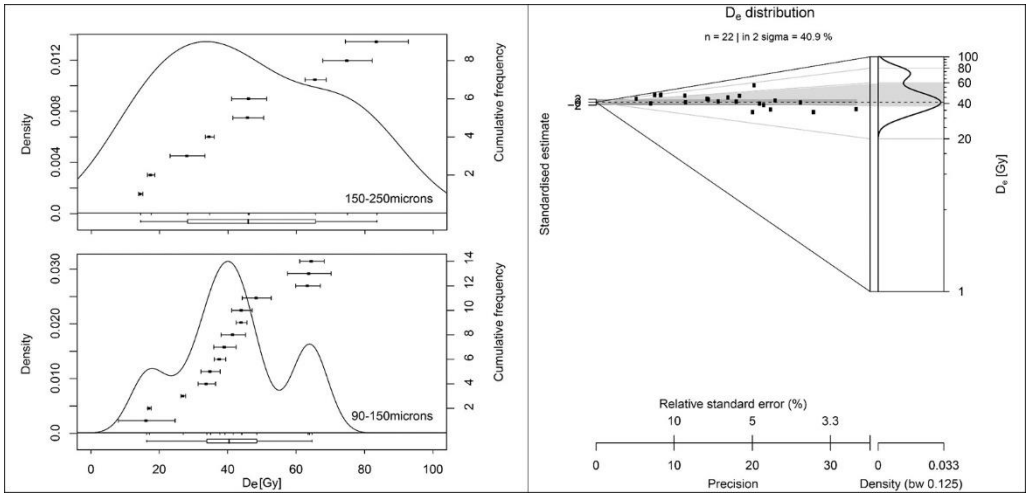

Figure S3. D_e distributions for CERSA286: left) Kernel Density Estimate Plot; right) Abanico Plot.

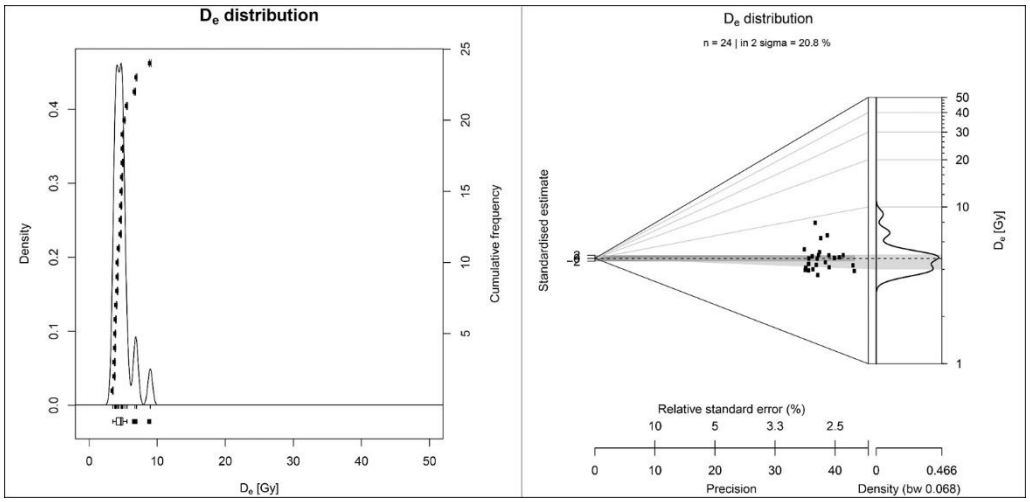

Figure S4. D_e distributions for CERSA288: left) Kernel Density Estimate Plot; right) Abanico Plot.

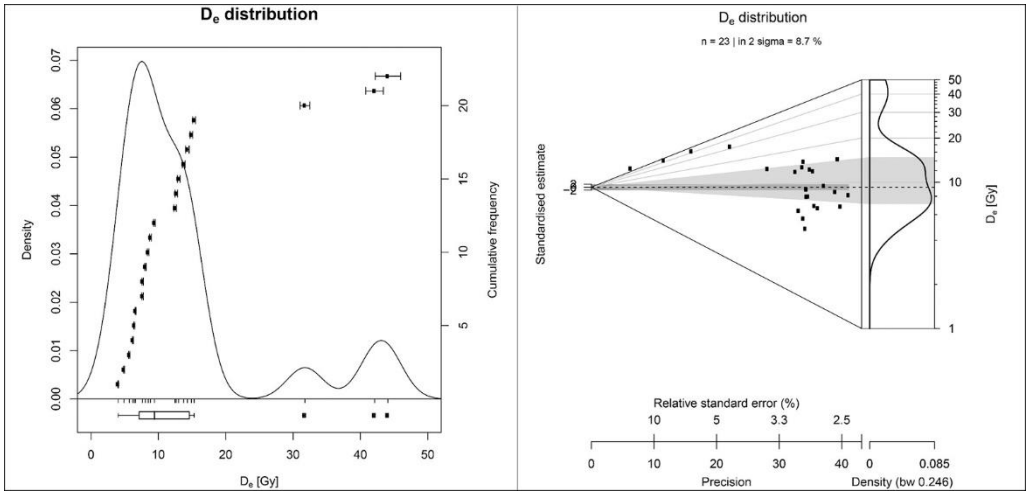

Figure S5. D_e distributions for CERSA289: left) Kernel Density Estimate Plot; right) Abanico Plot.

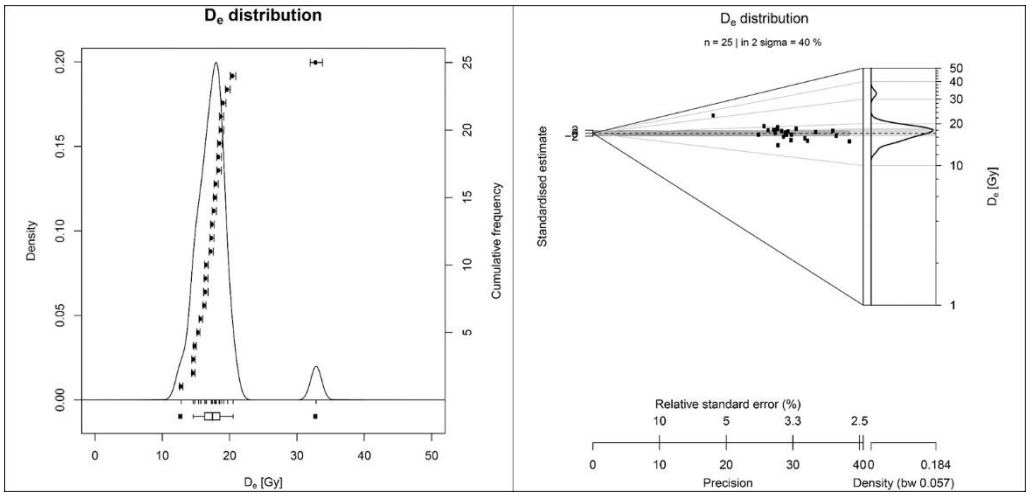

Figure S6. D_e distributions for CERSA300: left) Kernel Density Estimate Plot; right) Abanico Plot.

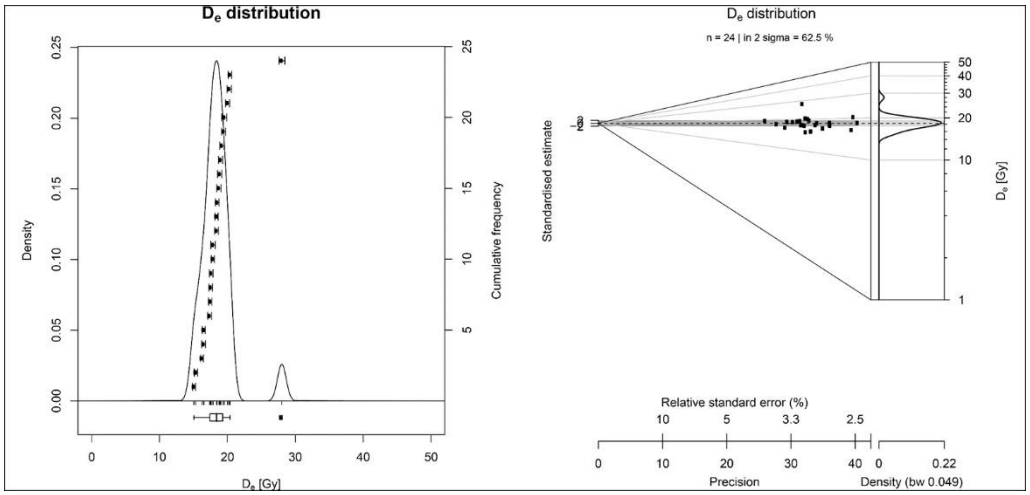

Figure S7. D_e distributions for CERSA301: left) Kernel Density Estimate Plot; right) Abanico Plot.

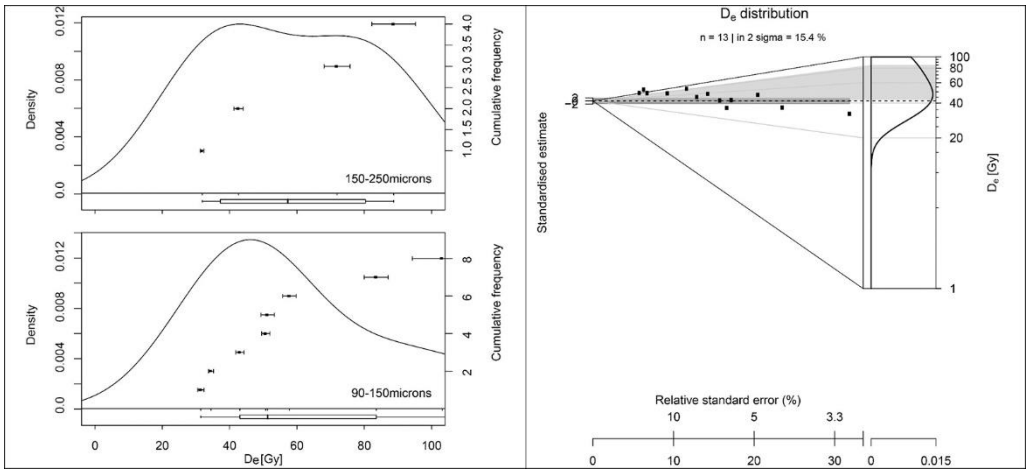

Figure S8. D_e distributions for CERSA302: left) Kernel Density Estimate Plot; right) Abanico Plot.

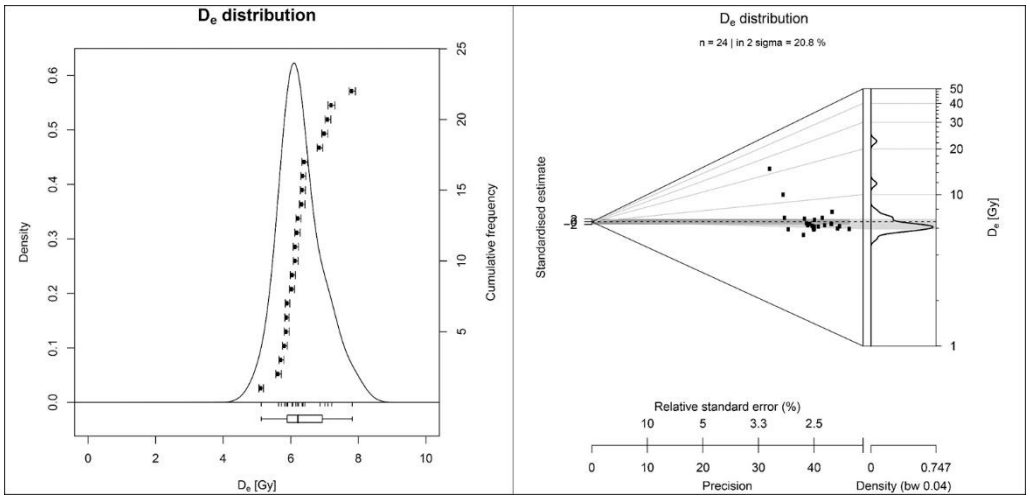

Figure S9. D_e distributions for CERSA303: left) Kernel Density Estimate Plot; right) Abanico Plot.

Radionuclide concentrations and environmental dose rates

The effective environmental dose rate to HF-etched quartz grain, $\dot{D}_{ex}$ consists of external gamma, $\dot{D}_{\gamma}$ beta, $\dot{D}_{\beta}$ and cosmic ray $\dot{D}_{c}$ contributions. $\dot{D}_{\alpha}$, $\dot{D}_{\gamma}$, $\dot{D}_{\beta}$ dose rates originate from naturally occurring radionuclides in the surrounding sediment matrix, including Potassium, *K* Uranium, *U* and Thorium, *Th* attenuated due to grain size and sediment-matrix water content. An internal dose rate, $\dot{D}_{in}$ due to K, U and Th inclusions within quartz, may add a negligible contribution to the total effective dose. The contribution from the cosmic dose, $\dot{D}_{c}$ is a function of geographic location (altitude, longitude and latitude) and burial depth, and is calculated from Prescott & Hutton (1994).

Dose rate measurements and determinations

Dose rate measurements were undertaken by High-Resolution Gamma Spectrometry (HRGS) at the Environmental Radioactivity Laboratory, in the School of Biological and Earth Sciences at the University of Stirling (UKAS Testing Lab 2751). All sample handling, processing and analysis were undertaken in accordance, and in compliance with ERL protocols LS03.1, 03.2 & 03.6 and LS08. The samples were sealed for four weeks prior to final counting. HRGS measurements were performed on a High Purity Germanium (HPGE) detector. Standard laboratory efficiency calibrations were used, derived from GE Heathcare Ltd QCY48 Mixed Radionuclide Spike and DKD RBZ-B44 ^{210}Pb spike. All absolute efficiency calibrations were corrected for variations in sample density and matrix. The decay reference date was the 11 June 2018.

Dose rate results

These data were used to determine infinite matrix dose rates for α, γ and β radiation (Table S4), using the conversion factors of Guérin *et al*. (2011), and grain-size attenuation factors of Mejdahl (1979). $\dot{D}_{\alpha}$, $\dot{D}_{\gamma}$, $\dot{D}_{\beta}$ dose rates derived from HRGS are listed in Table S5. External $\dot{D}_{\alpha}$ dose rates were ignored as the α irradiated portion of quartz was removed by HF-etching.

Table S4. Equivalent concentrations of K, U and Th determined by HRGS, together with infinite matrix dose rates for α, γ and β radiation.

CERSA no.	Radionuclide concentrations			Dose rates, Dry[a] / mGy a^{-1}		
	K / %	U / ppm	Th / ppm	$\dot{D}_{\alpha}$	$\dot{D}_{\beta}$[b]	$\dot{D}_{\gamma}$
285	4.27±0.27	6.79±0.27	18.1±0.9	32.4±1.0	4.41±0.22	2.69±0.09
286	4.56±0.28	7.44±0.27	14.0±0.7	31.1±0.9	4.62±0.23	2.64±0.08
288	3.66±0.24	6.24±0.26	13.0±0.8	27.0±0.9	3.78±0.2	2.23±0.08
289	3.44±0.24	5.83±0.28	14.3±0.9	26.9±1.0	3.59±0.19	2.19±0.08
300	3.47±0.23	5.96±0.24	13.9±0.8	26.9±0.9	3.63±0.19	2.20±0.07
301	3.56±0.24	5.43±0.27	14.6±0.9	26.0±1.0	3.64±0.20	2.19±0.08
302	3.35±0.23	6.54±0.3	15.8±1.0	29.9±1.1	3.65±0.19	2.32±0.08
303	3.43±0.22	6.19±0.25	13.8±0.8	27.5±0.92	3.62±0.18	2.21±0.07

[a] based on dose rate conversion factors in Guérin *et al*. (2011).

[b] attenuated for grain size based on Mejdahl (1979).

Table S5 lists the effective environmental dose rates to the 200µm HF-etched quartz grain, $\dot{D}_{ex}$, combining the derived $\dot{D}_{\beta}$ and $\dot{D}_{\gamma}$, attenuating these for grain size and water content, and an estimate for the cosmic dose contribution.

Table S5. Effective dose rates to the 150–250µm HF-etched quartz.

CERSA no.	Assumed water content (%)	Gamma dose rate (mGy a^{-1})	Effective Beta dose rate (mGy a^{-1})	Cosmic Dose rate contribution (mGy a^{-1})	Total effective dose rate (mGy a^{-1})
285	19±5	3.64±0.25	2.21±0.13	0.15±0.02	6.00±0.28
286	19±5	3.81±0.26	2.17±0.12	0.15±0.02	6.13±0.29
288	18±5	3.14±0.23	1.85±0.11	0.15±0.02	5.15±0.25
289	18±5	2.99±0.22	1.82±0.11	0.15±0.01	4.95±0.24
300	18±5	3.01±0.21	1.82±0.11	0.14±0.01	4.98±0.24
301	18±5	3.03±0.22	1.82±0.11	0.14±0.01	4.98±0.25
302	18±5	3.03±0.22	1.93±0.11	0.14±0.01	5.09±0.25
303	18±5	3.01±0.21	1.83±0.11	0.15±0.02	4.99±0.24

Table S6. Age determinations.

Field ID	CERSA lab code	Depth (m)	Stored dose (Gy)	Dose rate (mGy a^{-1})	Age (ka)	Age (years)
P1 OSL1	285	0.48	22.23±0.20 (0.63)	6.00±0.28	3.71±0.18	1690±180 BC†
P1 OSL2	286	0.50	19.23±1.06 (11.3)	6.13±0.29	3.14±0.23	1120±230 BC
P2 OSL1	288	0.35	4.37±0.03 (0.14)	5.15±0.25	0.85±0.04	AD 1170±40
P2 OSL2	289	0.70	7.08±0.05 (0.84)	4.95±0.24	1.43±0.07	AD 590±70
P2A OSL1	300	1.04	16.62±0.12 (0.43)	4.98±0.24	3.34±0.16	1320±160 BC
P2A OSL2	301	1.12	17.83±0.11 (0.33)	4.98±0.25	3.58±0.18	1560±180 BC
P2A OSL3	302	1.27	33.72±0.93 (10.49)	5.09±0.25	6.62±0.37	4600±370 BC*
P2A OSL4	303	0.50	6.19±0.03 (0.12)	4.99±0.24	1.24±0.06	AD 780±60

† low-dose tail to approximately 20 Gy, corresponding to sediment age of *c*. 1300–1400 BC.

* large D_e distributions; age calculated from low-dose population.

References

BURBIDGE, C.I., D.C.W. SANDERSON, R.A. HOUSLEY & J.P. ALLSWORTH. 2007. Survey of Palaeolithic sites by luminescence profiling: a case study from Eastern Europe. *Quaternary Geochronology* 2: 296–302. https://doi.org/10.1016/j.quageo.2006.05.024

DIETZE, M., S. KREUTZER, M.C. FUCHS, C. BUROW, M. FISCHER & C. SCHMIDT. 2013. A practical guide to the R package Luminescence. *Ancient TL* 32: 11–18.

GUÉRIN, G., N. MERCIER & G. ADAMIEC. 2011. Dose-rate conversion factors: update. *Ancient TL* 29: 5–8.

KINNAIRD, T., T.C. DAWSON, D. SANDERSON, D. HAMILTON, A. CRESSWELL & R. RENNELL. 2017a. Chronostratigraphy of an eroding complex Atlantic round house, Baile Sear, Scotland. *Journal of Coastal and Island Archaeology* 14. https://doi.org/10.1080/15564894.2017.1368744

KINNAIRD, T., J. BOLÒS, A. TURNER & S. TURNER. 2017b. Optically-stimulated luminescence profiling and dating of historic agricultural terraces in Catalonia (Spain). *Journal of Archaeological Science* 78: 66–77. https://doi.org/10.1016/j.jas.2016.11.003

MEJDAHL, V. 1979. Thermoluminescence dating: Beta-dose attenuation in quartz grains. *Archeometry* 29: 61–72. https://doi.org/10.1111/j.1475-4754.1979.tb00241.x

MUNOZ-SALINAS, E., P. BISHOP, D.C.W. SANDERSON & T.C. KINNAIRD. 2014. Using OSL to assess hypotheses related to the impacts of land-use change with the early nineteenth century arrival of Europeans in south-eastern Australia: an exploratory case study from Grabben Gullen

Creek, New South Wales. *Earth Surface Processes and Landforms* 39: 1576–86. https://doi.org/10.1002/esp.3542

MURRAY, A.S. & A.G. WINTLE. 2000. Luminescence dating of quartz using an improved single-aliquot regenerative-dose protocol. *Radiation Measurements* 32: 57–73. https://doi.org/10.1016/S1350-4487(99)00253-X

PRESCOTT, J.R. & J.T. HUTTON. 1994. Cosmic ray contributions to dose rates for luminescence and ESR dating: large depths and long-term time variations. *Radiation Measurements* 23: 497–500. https://doi.org/10.1016/1350-4487(94)90086-8

SANDERSON, D.C.W. & S. MURPHY. 2010. Using simple portable OSL measurements and laboratory characterisation to help understand complex and heterogeneous sediment sequences for luminescence dating. *Quaternary Geochronology* 5: 299–305. https://doi.org/10.1016/j.quageo.2009.02.001

TURNER, S., J. BOLÒS & T. KINNAIRD. 2018. Changes and continuities in a Mediterranean landscape: a new interdisciplinary approach to understanding historic character in western Catalonia. *Landscape Research* 43: 922–38. https://doi.org/10.1080/01426397.2017.1386778